XIE, F., WANG, S., XIE, Y., FERNANDEZB, C., LI, X. and ZOU, C. 2020. A novel battery state of charge estimation based on the joint unscented kalman filter and support vector machine algorithms. *International journal of electrochemical science* [online], 15(8), pages 7935-7953. Available from: https://doi.org/10.20964/2020.08.83.

A novel battery state of charge estimation based on the joint unscented kalman filter and support vector machine algorithms.

XIE, F., WANG, S., XIE, Y., FERNANDEZB, C., LI, X. and ZOU, C.

2020

Int. J. Electrochem. Sci., 15 **(2020)** 7935 – 7953, doi: 10.20964/2020.08.83

International Journal of
ELECTROCHEMICAL
SCIENCE
www.electrochemsci.org

A Novel Battery State of Charge Estimation Based on the Joint Unscented Kalman Filter and Support Vector Machine Algorithms

Fei Xie[1], *Shunli Wang*[1,*], *Yanxin Xie* [1], *Carlos Fernandezb*[2], *Xiaoxia Li*[1], *Chuanyun Zou*[1]

[1] School of Information Engineering, Southwest University of Science and Technology, Mianyang 621010, China;
[2] School of Pharmacy and Life Sciences, Robert Gordon University, Aberdeen AB10-7GJ, UK.
[*]E-mail: wangshunli@swust.edu.cn

Received: 5 January 2020 / *Accepted:* 12 February 2020 / *Published:* 10 July 2020

With the development of new energy sources becoming the mainstream of energy development strategies, the role of electric vehicle-powered lithium-ion batteries in the field of automobile transportation is becoming more and more obvious. An efficient the Battery Management System is necessary for the real-time usage monitor of each battery cell, which analyzes the battery status to ensure its safe operation. A complex equivalent circuit model is proposed and established. the Improved Equivalent Circuit Model is used to realize the precise mathematical expression of the power lithium-ion battery packs under special conditions. The State of Charge estimation method which is based on Unscented Kalman Filter has a good filtering effect on the nonlinear systems. Based on the State of Charge estimation of Support Vector Machine, the samples in the nonlinear space of lithium-ion battery are mapped to the linear space. It can be seen from the experimental analysis that a joint Unscented Kalman Filter and Support Vector Machine algorithms for State of Charge estimation has higher accuracy. The experimental results show that the tracking error is less than 1.00%.

Keywords: Battery Management System; State of Charge; Improved Equivalent Circuit Model; Unscented Kalman Filter; Support Vector Machine

1. INTRODUCTION

Under the severe situation of global energy shortage, the energy supply model cannot last for a long time. Seeking a sustainable economic development and developing new energy industry has become the fundamental means to solve the problem. In the new energy industry, Electric Vehicles (EVs) have become the hotspot of social research because of their environmental characteristics to meet the high-efficiency and low-carbon economy of human society. In recent years, due to the excellent

performance of the Lithium-Ion Battery (LIB) itself, it has become the preferred power supply for new EVs. The researchers reviewed LIBs for EVs at low temperatures [1]. During the entire life cycle of the LIB, the monitoring and adjustment of the core parameter State of Charge (SOC) by the Battery Management System (BMS) will affect the effectiveness and safety of the emergency power output. The BMS is a necessary part of the power LIB packs, in which the SOC is a very important factor that affects its performance. Because the working characteristics of the LIB pack are highly nonlinear, the SOC value cannot be measured directly. Therefore, the accurate SOC estimation has become the focus and difficulty of the BMS design.

To build a precise SOC estimate for the BMS, the researchers conducted model-based real-time SOC and State of Health (SOH) evaluations [2-12]. The LIB state estimation of EVs based on the Neural Network (NN) method [10, 13-15]. The real-time SOC estimation was achieved by constructing a robust adaptive sliding mode observer [13, 16-18]. Based on the State of Balance (SOB) estimation, the online dynamic balance management of the LIBs were realized [19]. Joint estimation of the EV power battery SOC was constructed by using the least squares method and the Kalman Filter (KF) algorithm [20]. In the SOC estimation process, a dynamic system model was obtained based on the Extended Kalman Filter (EKF) algorithm to avoid estimating the occurrence of failure phenomena. Many researchers based on the KF algorithm and improved it to achieve EV SOC estimation [20-23]. The optimal transmission strategies were introduced for the two-user energy harvesting device networks with limited SOC knowledge [24].Analysis of Power LIB packs affected by environmental and aging factors [25-27]. An advanced machine learning method was proposed for the LIB state estimation of the EVs [28, 29]. Combining the data-driven and model-based system residual life prediction methods, a hybrid framework was constructed [30].

SOC estimation of LIBs allows the BMS to run accurately and efficiently [31]. For the research of this subject, the SOC estimation research scheme combining Unscented Kalman Filter (UKF) and SOC algorithm is creatively constructed. From another angle, the SOC estimation of LIBs is compared with the independent UKF algorithm. The experimental results show that after the introduction of Support Vector Machine (SVM) algorithm, the combination of UKF and SVM algorithm can effectively improve the accuracy of SOC estimation and provide a new idea for estimating SOC.

2. EQUIVALENT CIRCUIT MODELING

Aiming at the accurate mathematical simulation expression of the operating characteristics in the power LIB pack, the equivalent circuit modeling (ECM) analysis was explored to study the construction method of its equivalent model [32]. The LIB packs consist of multiple cells cascaded to achieve high power applications and provide the needed energy. Analysis of issues of integrating LIB pack into EVs [27, 33]. In order to adapt to the challenging environment of EV safety power supply applications, a novel ECM construction method is proposed. Assuming that all cells in the LIB module are the same, by introducing SOB into the internal LIB cells and considering the inconsistency of the batteries, an equivalent model of the improved equivalent circuit model (IECM) is proposed and applied to the SOC estimation process of the power LIB packs.

2.1. Internal resistance model construction

Considering the working characteristics of the battery, the internal resistance model of the battery is established and applied to the experimental SOC estimation method [34]. This model not only has the characteristics of simple structure, but also can be used as the basis of other equivalent models. In this model, the internal equivalent structure of the battery is characterized by voltage source and internal resistance. the internal equivalent structure as shown in Figure 1.

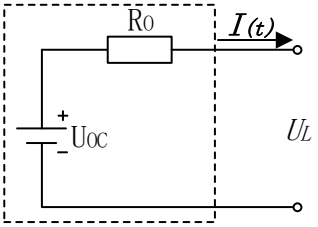

Figure 1. Internal resistance equivalent diagram

In the Figure 1, U_{OC} represents the open circuit voltage of the battery, which is a constant value; R_O represents the ohmic resistance of the battery; U_L represents the terminal voltage at both ends of the battery. In this model, both U_{OC} and R_O were set as fixed values, which was too simplified to be consistent with the change of parameters in the actual operation of the battery, and ignored the fact that the internal resistance of the battery changed with the change of electrolyte concentration. Therefore, this model is not suitable for SOC estimation of actual lithium ion batteries because of its low accuracy.

2.2. Thevenin model construction

An improvement over the Internal resistance model is the addition of a RC circuit, which is used to characterize the polarization effect of lithium-ion batteries in operation. the Thevenin model structure [35] as shown in Figure 2

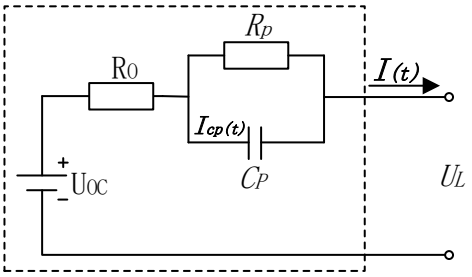

Figure 2. Thevenin equivalent diagram

Where U_{OC} represents the open circuit voltage of the battery, R_O represents the ohmic internal resistance of the battery, and R_P and C_P respectively represent the polarization internal resistance and polarization capacitance inside the battery. The Thevenin model can better represent the dynamic response of the battery. R_O can represent the instantaneous change of the battery voltage response at the

moment of charge and discharge, and RC circuit can reflect the gradual change of battery voltage during and after charge and discharge, such as sliding or lifting. The simulation accuracy of Thevenin model is much higher than that of internal resistance model, and the complexity of the model is not high.

2.3. PNGV model construction

PNGV model adds a large storage capacitor C_b to Thevenin model [36], as shown in Figure 3. C_b represents the change in the open circuit voltage of the battery resulting from the accumulation of load current.

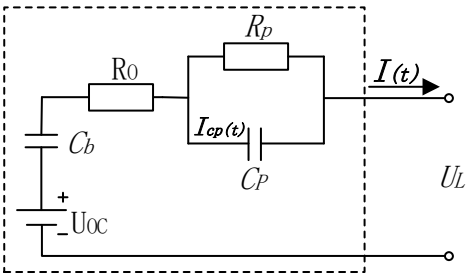

Figure 3. PNGV model diagram

The nonlinearity of PNGV model is very typical, and it also has the characteristics of Thevenin model. At the same time, the energy storage capacitor is also added, which enables the PNGV model to reflect the steady-state changing battery voltage, so that the battery characteristics can be more accurately represented and the accuracy improved accordingly. Because the structure of the PNGV model is more complex, the number of parameters to be identified in the model is more difficult than that of Thevenin model.

2.3. Improved equivalent circuit model

An improved equivalent circuit model method, IECM, is proposed. This method considers the accuracy of the feature description and the computational complexity, and can accurately describe the working state of the LIB pack of EVs. The first proposed IECM equivalent model adds parallel resistance to the first-order RC equivalent to characterize the self-discharge effect. Secondly, based on the PNGV equivalent model, the IECM model introduces a reverse diodes resistance parallel circuit to characterize the difference in internal resistance during charging and discharging. Finally, based on the Thevenin equivalent model, the IECM equivalent model adds a series power supply and resistance to the electromotive force to characterize the influence of the equilibrium state, and comprehensively and accurately describes the working process of the LIB pack. The structure is shown in Figure 4.

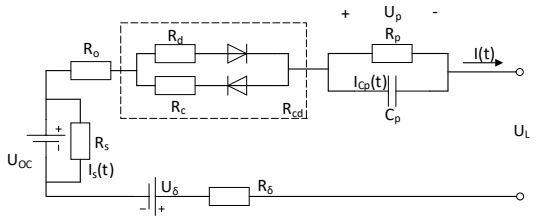

Figure 4. The improved equivalent model of IECM

In the IECM model shown in Figure 4, the meaning of each parameter is as follows. U_{OC} represents the OCV value of the power LIB pack. The R_S resistance is large and is intended to characterize the self-discharge effect. R_o represents Ohmic resistance of the battery, which characterizes the voltage drop between the positive and negative electrodes during the Discharging and Charging Maintenance(DCM) process. The proposed IECM model uses a first-order RC network to simulate the relaxation effects of the LIB pack, and attains its transient response characteristics of the LIB pack. The R_P and C_P parallel circuit reflects the generation and elimination of polarization effects, where R_P is polarization resistance and C_P is polarization capacity. R_d is the discharge resistance of the discharge period, which characterizes the resistance difference during the discharging process of the power LIB pack. R_c is a charging resistor that characterize the difference in resistance during discharging. U_δ and R_δ are used to characterize the effect of the equilibrium state between the interconnected monomers. U_L represents the terminal voltage between the positive and negative terminals of the power LIB pack connected to the external circuit during the charge and discharge process. I_L represents the inflow or outflow current value of the power LIB pack connected to the external circuit. In the model, the OCV is represented as a constant voltage source in which the Ohmic internal resistance, capacitance, and resistance are connected in parallel to describe the potential of the circuit. Indicates the load voltage of the battery, indicating the load current of the battery pack. According to the model and Kirchhoff's law, the relationship between the voltages of the various components of the circuit can be described.

2.4. State-space mathematical description

When the LIB pack is in a charging or discharging state, the specified discharge current direction is positive. According to the equivalent circuit model of the battery of Figure 4, the following equations can be obtained.

$$\begin{cases} U_{OC}(t) = I_s(t) R_s \\ U_p(t) = I(t) R_p \left(1 - e^{-T_s/R_p C_p}\right) \\ U_L(t) = \left(U_{OC} - U_\delta\right) - \left(R_o + R_\delta\right) I(t) - U_p - I(t) R_{cd} \end{cases}$$

Where R_{cd} characterizes the internal resistances R_d and R_c at the time of charge and discharge. When the power lithium battery pack is in the discharge process, the value of R_{cd} is set to R_d; when it is charged, $R_{cd} = R_c$. The τ is the time constant of the RC parallel circuit in the equivalent circuit model, and its calculation expression is $\tau = R_P C_P$. T_s is the sampling time interval constant.

Considering the influence of the self-discharge internal resistance R_s, the state-space equation in the continuous time-state-space equation is established, as shown in Equation 2-1.

$$SOC(t) = SOC(0) - \int_0^t \frac{\eta_I \eta_T I(\tau)}{Q_n} d\tau - \int_0^t \frac{I_s(\tau)}{Q_n} d\tau \quad (2\text{-}1)$$

In the above expression, $SOC(t)$ represents the SOC value at time t, and $SOC(0)$ represents the SOC value at the initial time. η_I denotes the coulombic efficiency at different current I. η_T shows the effect of different temperature T on the coulomb efficiency η. Q_n is the rated capacity of the LIB pack.

Since the data acquisition and processing are in discrete time form during the actual calculation process, the state equation is discretized. Combining the state equation with the observation equation, the state space equation required to construct the SOC estimation is shown in equation (2).

$$\begin{cases} SOC(k \mid k-1) = SOC(k-1) - \dfrac{\eta_I \eta_T I(k) T_s}{Q_n} - K_s T_s \\ U_L(k) = (U_{OC} - U_\delta) - (R_o + R_\delta) I(k) - I(k) R_p \left(1 - e^{-T_s/(R_p C_p)}\right) - I(k) R_{cd} \end{cases}$$

3. RESEARCH ON SOC ESTIMATION METHOD

3.1. The definition of SOC

Currently, SOC estimation is achieved through a basic ampere-time integration method. The method is mainly used for the external feature representation of the system, that is, mainly monitoring the remaining power inside the battery at different times, which is very sensitive to the initial value of the SOC, and closely related to the SOC value of the previous moment. The working principle model of Ampere-hour(Ah) integral[37] is as follows:

$$SOC(k+1) = SOC(k) + \int_k^{k+1} \eta I(t) dt \quad (3\text{-}1)$$

Where $SOC(k)$ is the charge and discharge state of the previous moment; $SOC(k+1)$ is the remaining charge of the LIB at the current time; I is the instantaneous current of the LIB (the discharge state is negative, the state of charge is positive); η is the coulomb efficiency coefficient.

3.2. SOC estimation method based on UKF

UKF is a process that combines hidden Markov model with Bayes' theorem. For the nonlinear model, the Unscented Transformation (UT) is used to approximate the Gaussian distribution through a series of fixed number of sampling points, and the mean and variance of each probability distribution of the output variable are obtained. EKF needs to translate the problem into a linear Gaussian model [38, 39], while UKF can directly deal with nonlinear systems, eliminating the effects of linear errors and reducing computational complexity. Since the approximation accuracy of the UT to the statistical moment is high, the error only exists in the second order and above, and the influence can reach the influence of the second order EKF. Therefore, the UKF is used to realize the SOC estimation of the LIB. Using Taylor series expansion, pointless transformation and function fitting approximation, the mathematical description methods under different working conditions are explored, and the SOC

estimation model with parameter correction and adaptive adjustment ability is constructed. The basic idea of the establishment process is obtained after several cycles of testing, and the relationship between terminal voltage and time is obtained, as shown in Figure 5.

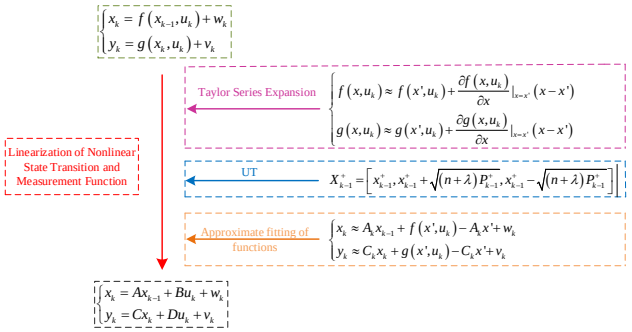

Figure 5. SOC estimation model construction of the power LIB pack

According to the SOC estimation accuracy target, the nonlinear characteristics of the power LIB pack are described based on UT process, which effectively avoids the estimation error caused by the Taylor series expansion and the abandonment of the high-order terms [40] . Compared with the Taylor series expansion method, the processing based on the UT has at least second-order precision, especially for the Gaussian distribution method to achieve third-order accuracy. The selection of the unscented transformed sampling points is based on the correlation sequence of the a prior mean and the square root of the a priori covariance matrix.

The UT exhibits good performance during the SOC estimation process, but if the stability of the linear processing in a small period cannot last for an effective period, it will result in a relatively poor estimation effect. According to the proportional symmetric sampling strategy, the transformed Sigma data points are obtained by nonlinear function transformation, and the transformed mean and covariance are obtained by weighting the data points, and then the weighting factors are obtained [41]. Assume that the system function is:

$$y = f(x) \tag{3-2}$$

The system inputs the random vector x, the dimension is n, $\overline{x}$ and P_x are the mean and covariance of the system input respectively; the system outputs the random variables y, $\overline{y}$ and P_y are the mean and covariance of the system output, respectively.

① Obtain the transformed Sigma data points.

$$x_0 = \overline{x} \tag{3-3}$$

$$x_i = \begin{cases} x_0 + \left(\sqrt{(n+\lambda)P_x}\right)_i, i = 1,\ldots,n \\ x_0 - \left(\sqrt{(n+\lambda)P_x}\right)_i, i = n+1,\ldots 2n+1 \end{cases} \tag{3-4}$$

② Sigma data points weighting.

$$\begin{cases} \sum_{i=0}^{2n} w_i = 1 \\ w_o^m = w_i^m = w_i^c = \lambda/(n+\lambda) \\ w_o^c = \lambda/(n+\lambda) + (1+\beta-\alpha^2) \end{cases} \quad (3\text{-}5)$$

Among them, λ is the proportional coefficient, which determines the distance between the Sigma point and the input mean of the system; w^m and w^c are the weighted coefficients required for the mean and variance of the Sigma point; α is the proportional scaling factor of the positive value, which is used to determine the distribution of the Sigma point; β is the parameter introducing the higher order information of the state transition equation of the nonlinear system, which is generally set to 2.

③ Get the mean and covariance of y.

$$\bar{y} = \sum_{i=0}^{2n} w_i^m y_i \quad (3\text{-}6)$$

$$P_y = \sum_{i=0}^{2n} w_i^c (y_i - \bar{y})(y_i - \bar{y})^T \quad (3\text{-}7)$$

Based on the Kalman estimation method with feedback regulation ability [40], in a nonlinear system, the real-time observations are superimposed to correct it. As shown in Figure 6.

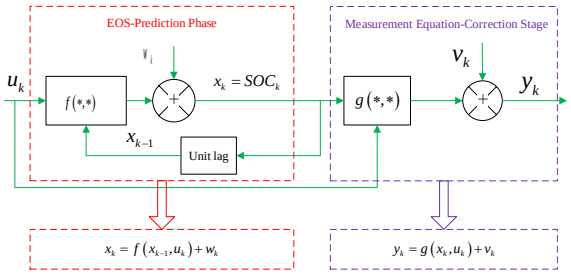

Figure 6. SOC estimation model framework for power LIB

In the estimation process, the equation of state and the equation of observation are shown as follows.

$$\begin{cases} x_k = f(x_{k-1}, u_k) + w_k \\ y_k = g(x_k, u_k) + v_k \end{cases} \quad (3\text{-}8)$$

In the formula, u_k is the input of the system, x_k is the state variable of the system, y_k is the measurement signal. w_k and v_k are the process noise and observation noise at k time, respectively, the covariances are Q_k and R_v, respectively.

1) Initial value calculation:

$$\begin{cases} \bar{x} = E(x_0) \\ p_0 = E(x_0 - \bar{x})(x_0 - \bar{x})^T \end{cases} \quad (3\text{-}9)$$

2) Establish Sigma Point:

$$x_{k-1}^{i}=\begin{cases}\overline{x}_{k-1}+\left[\sqrt{(L+\lambda)\,p_{k-1}}\right]_i, i=1,...,L\\ \overline{x}_{k-1}-\left[\sqrt{(L+\lambda)\,p_{k-1}}\right]_i, i=L+1,...,2L+1\end{cases} \quad (3\text{-}10)$$

3) State renewal equation:

$$\begin{cases}x_{k|k-1}^{i}=f\left(x_{k-1}^{i}\right), \overline{x}_{k}^{-}=\sum_{i=0}^{2L}\omega_i^{m}x_{k|k-1}^{i}\\ p_{k|k-1}=\sum_{i=0}^{2L}\omega_i^{c}\left(x_{k|k-1}^{i}-\overline{x}_{k}^{-}\right)\left(x_{k|k-1}^{i}-\overline{x}_{k}^{-}\right)^{T}+Q_k\\ y_{k|k-1}^{i}=g\left(x_{k|k-1}^{i}\right), \overline{y}_{k}^{-}=\sum_{i=0}^{2L}\omega_i^{m}\left[g\left(x_{k|k-1}^{i}\right)+v_{k-1}^{i}\right]=\sum_{i=0}^{2L}\omega_i^{m}y_{k|k-1}^{i}\end{cases} \quad (3\text{-}11)$$

$k|k-1$ in the formula is an estimate of k-time based on $k-1$-time.

4) The measurement update equation is as follows:

$$\begin{cases}p_{\overline{y},k}=\sum_{i=0}^{2L}\omega_i^{c}\left(y_{k|k-1}^{i}-\overline{y}_{k}^{-}\right)\left(y_{k|k-1}^{i}-\overline{y}_{k}^{-}\right)^{T}+Q_k\\ p_{\overline{xy},k}=\sum_{i=0}^{2L}\omega_i^{c}\left(x_{k|k-1}^{i}-\overline{x}_{k}^{-}\right)\left(y_{k|k-1}^{i}-\overline{y}_{k}^{-}\right)^{T}\\ K=p_{\overline{xy},k}{p_{\overline{y},k}}^{-1}, \overline{\mathrm{x}}_{k}=\overline{\mathrm{x}}_{k}^{-}+K\left(y_k-\overline{y}_{k}^{-}\right), p_{k|k}=p_{k|k-1}-Kp_{\overline{y},k}K^{T}\end{cases} \quad (3\text{-}12)$$

5) Repeat the above four steps.

3.3. SOC estimation method based on SVM

The function of SVM that is a kind of two classification model is to find a hyperplane to segment samples. The principle of segmentation is to maximize the interval, which is finally transformed into a convex quadratic programming problem to solve. The models from simple to complex include: (1) When the training samples are linearly separable, a linear separable support vector machine is learned by maximizing the hard interval; (2) When the training samples are approximately linearly separable, a linear support vector machine is learned by maximizing the soft interval; (3) When the training samples are not separable linearly, a nonlinear support vector machine is learned by kernel technique and soft interval maximization.

Structural risk minimization (SRM) is a strategy to prevent over fitting. It refers to the construction of function set into a sequence of function subsets, so that the subsets are arranged according to the size of VC dimension. The minimum empirical risk is found in each subset, and the empirical risk and confidence range are considered in the trade-off between subsets to minimize the actual risk.

Formula by generalization error bounds:

$$R(w)\le \mathrm{Re}\,mp(w)+\phi\left(n/h\right) \quad (3\text{-}13)$$

Among them, $R(w)$ is the real risk, $\mathrm{Re}\,mp(w)$ is the experience risk and $\phi\left(n/h\right)$ is the confidence risk. Knowing the actual error $R(w)$ is:

$$1-\eta \le R(w)\le \frac{1}{l}\sum_{i=1}^{l}Lf[y_i,f(x_i,w)]+\sqrt{\frac{n[\ln(l/2)+1]-\ln(\eta/4)}{l}} \quad (3\text{-}14)$$

Where $0 \le \eta \le 1$ and $\frac{1}{l}\sum_{i=1}^{l} Lf[y_i, f(x_i, w)]$ are empirical risk formulas, n is VC dimensions of learning machines and l is sample numbers. Confidence risk is related to two quantities. One is the sample size. Obviously, the larger the given sample size, the closer our learning results approximate the correct value, the smallest the confidence risk. The other is the VC dimension of the classification function. Obviously, the larger the VC dimension, the poorer the generalization ability, the greater the confidence risk.

The so-called VC dimension refers to a set of index functions. If there are h samples that can be separated by all possible types of functions in the function set, then the function set can scatter h samples; the VC dimension of the function set is the maximum number of samples that it can break up h. If there are functions that can scatter any number of samples, the VC dimension of the set of functions is infinite, and the VC dimension of bounded real functions can be defined by converting it into an indicator function with a certain threshold value. In order to estimate the indication function, it is transformed into a regression problem, and the ε insensitive loss function is used to SVM classification algorithm to predict the empirical risk [42] . By loss function:

$$L(y, f(x)) = (1 - yf(x))_+ \qquad (3\text{-}15)$$

Then,

$$c[y - f(x), x] = |y - f(x)|_\varepsilon = \begin{cases} 0, |y - f(x, w)| \le \varepsilon \\ |y - f(x, w)| - \varepsilon, others \end{cases} \qquad (3\text{-}16)$$

Introduce a nonlinear mapping function, map the original model space to the higher-dimensional feature space Z, construct the optimal classification hyperplane in the feature space, and use the linear function set in the feature space.

$$f(x) = w\varphi(x) + b \qquad (3\text{-}17)$$

The linear problem in high-dimensional space corresponds to the non-linear problem in low-dimensional space and is transformed into a regression problem. The effect of non-linear regression in original space is obtained, thus realizing the classification of the original mode space.

For a given training data set, its constrained optimization problem is:

$$\min \frac{1}{2}\|w\|^2 + c\sum_{i=1}^{l}(\xi_{i1} + \xi_{i2}) \qquad (3\text{-}18)$$

And satisfy

$$\begin{cases} y_i - w\varphi(x_i) - b \le \xi_{i1} + \varepsilon \\ w\varphi(x_i) - b - y_i \le \xi_{i2} + \varepsilon \\ \xi_{i1} \ge 0, \xi_{i2} \ge 0 \\ i = 1, 2 \ldots l \end{cases} \qquad (3\text{-}19)$$

Known by Lagrange Multiplication (LM):

$z = f(x, y)$ possible extreme point under condition $\varphi(x, y) = 0$, constructor

$$F(x, y) = f(x, y) + \lambda\varphi(x, Y) \qquad (3\text{-}20)$$

$$\text{s.t.} \quad \begin{cases} f_x(x,y) + \rho\varphi_x(x,y) = 0 \\ f_y(x,y) + \rho\varphi_y(x,y) = 0 \\ \varphi(x,y) = 0 \end{cases} \qquad (3\text{-}21)$$

If it is established, (x,y) is the best possible extremum. Therefore,

$$\begin{aligned} &\max_{\alpha_{i1},\ \alpha_{i2},\ \beta_{i1},\ \beta_{i2}} \min_{w,b,\xi} \{Lp \\ &= \min \frac{1}{2}\|w\|^2 + c\sum_{i=1}^{l}(\xi_{i1} + \xi_{i2}) \\ &-\sum_{i=1}^{l}\alpha_{i1}[\xi_{i1} + \varepsilon - y_i + w\varphi(x_i) + b] \\ &-\sum_{i=1}^{l}\alpha_{i2}[\xi_{i2} + \varepsilon + y_i - w\varphi(x_i) - b] \\ &-\sum_{i=1}^{l}(\xi_{i1}\beta_{i1}, \xi_{i2}\beta_{i2})\Big\} \end{aligned} \qquad (3\text{-}22)$$

When $\frac{\partial L}{\partial w} = 0$, the extreme value is available.

$$w = \sum_{i=1}^{l}(\alpha_{i1} - \alpha_{i2})\varphi(x_i) \qquad (3\text{-}23)$$

Substituting w into the estimation function yields a regression estimation expression of:

$$f(x, \alpha_{i1}, \alpha_{i2}) = \sum_{i=1}^{l}(\alpha_{i1} - \alpha_{i2})\varphi(x_i)\varphi(x_j) + b \qquad (3\text{-}24)$$

Let $k(x_i, x_j) = \varphi(x_i)\varphi(x_j)$ be a Kernel Function (KF).

$$k(x_i, x_j) = \exp(-\gamma |x_i - x_j|^2) \qquad (3\text{-}25)$$

The KF is to be able to map samples in a nonlinear space into a linear space. LIB is a highly nonlinear system that can be transformed into a linear problem by KF and solved by calculation [37]. It is an important solution of SVM for nonlinear inseparable problems. The necessary condition for an effective KF k is that the KF matrix k is symmetrically positive semidefinite. If it satisfies Mercer theorem, it can generally be selected as a KF.

After the test process, it is known that there are current, voltage and other factors affecting the SOC value of LIBs. Therefore, these variables with nonlinear changes are taken as input parameters. However, after a large amount of experimental data calculation, it is found that the error is gradually increasing. Slowly, it is found that the historical parameters of the SOC of LIBs have a great impact on the estimation, so it is included in the selection of input variables.

3.4. Estimation of SOC Based on UKF and SVM Joint Algorithms

The output of UKF algorithm is used as the input of SVM algorithm to estimate SOC twice, to improve the estimation accuracy. The system structure block diagram is shown in Figure 7.

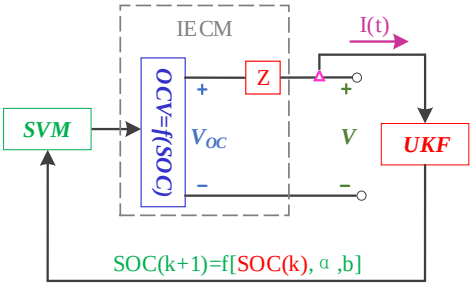

Figure 7. The structural of the UKF and SVM joint algorithm

As shown in the figure above, α is the weight of the corresponding kernel function in the SVM algorithm. The SOC value estimated by the UKF algorithm is taken as an initial condition of the SVM, that is, the SOC of the previous moment. Through the above described method, the working characteristics of the LIB are obtained, which has high practical value.

4. EXPERIMENTAL ANALYSIS

4.1. Battery test bench

The battery test bench structure is shown in Figure 8, which is consists of: (1) The experimental battery; (2) The battery testing system (NEWARE BTS-4000) used to load the battery controlled by the host computer with programmable current. And this apparatus can detect the voltage, current and temperature of the battery with the sampling interval is 1s; (3) The temperature chamber (TT-5166TH-7) that programed by the host computer to provide the constant temperature environment (25℃) for the battery; (4) Host computer that is used to control and communicate with other apparatuses with TCP/IP protocol.

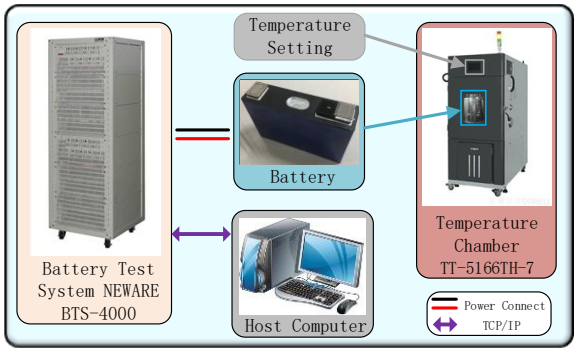

Figure 8. Battery test bench

4.2. The HPPC test of parameter identification

The hybrid pulse power characteristic(HPPC) test is used for parameter identification. The test is carried out with $LiMn_2O_4$ battery with a nominal capacity of 12Ah. The parameters of the battery are given in Table 1.

Table 1. Parameters of the LiMn2O4 battery

Parameters	Nominal capacity	Lower cut-off voltage	Upper voltage limits	Operating temperature
Value	12Ah	2.75	4.25	-20℃to40℃

The parameters that need to be identified in the equivalent circuit model include U_{OC}, R_S, R_o, R_P, C_P , R_d, R_c and OCV-SOC characteristic curves. The experimental conditions and process were as follows: 0.2 C constant current discharge at ambient temperature of 25 ° C for 3 min, and then allowed to stand for 40 min until the battery SOC was 0. The specific process is shown in Figure 9, and the OCV-SOC curve is shown in Figure 10.

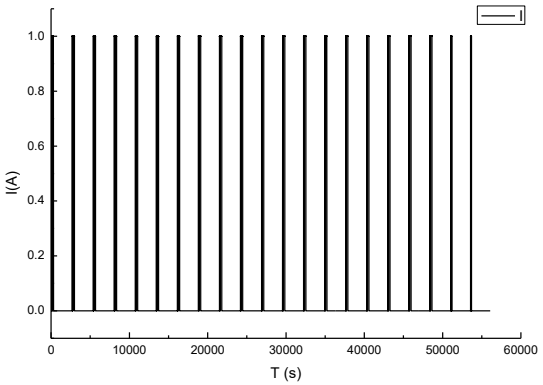

Figure 9. Current profile of OCV-SOC

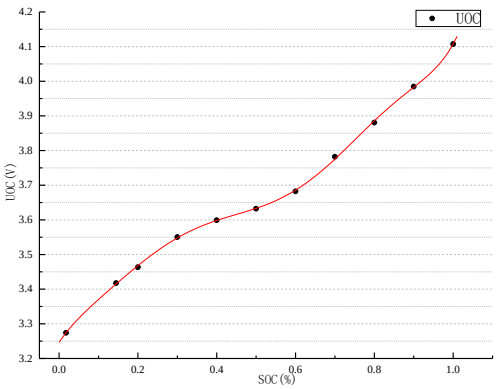

Figure 10. The curve of OCV-SOC

The state equation of lithium-ion battery is expressed by polynomial fitting based on the data of voltage drop at the moment of power-off or the voltage at the moment of power-on by curve fitting. By comparing and analyzing the fitting effect of polynomials of different degrees, the quantic polynomials are selected for fitting, and the corresponding ohmic internal resistance values under different SOC are obtained [36]. The ohmic internal resistance identification curve is shown in Figure 11.

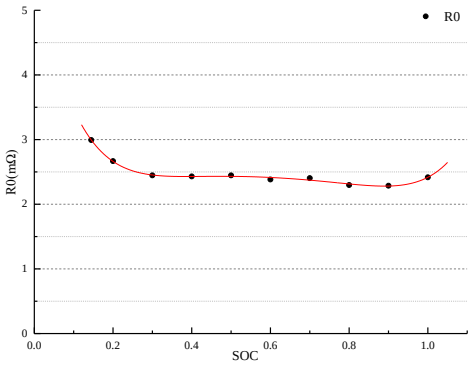

Figure 11. The identification curve of R_o

The parameters of the RC network can be identified by nonlinear fitting of the zero input data of the battery stationary stage and the closed loop analysis of the battery output voltage. The R_P and C_P is shown in Figure 12 and Figure 13.

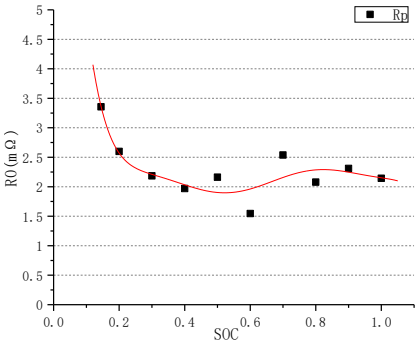

Figure 12. The identification curve of R_P

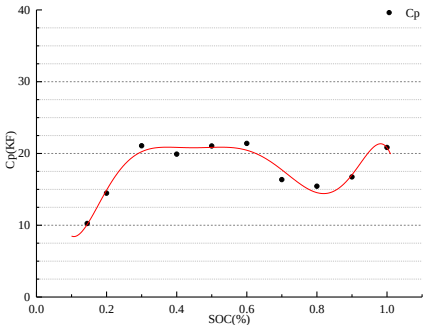

Figure 13. The identification curve of C_P

Through the analysis of the parameter identification process and principle, the model is constructed, and the general knowledge of covariance and noise is pre-set as known conditions, and taken into the additional consideration in the belonging sub-module. After the state space equation structure of the LIB pack is established, its coefficients need to be determined experimentally. The parameter identification equations and processes are implemented in a separate parameter identification module [39], as shown in Figure 14.

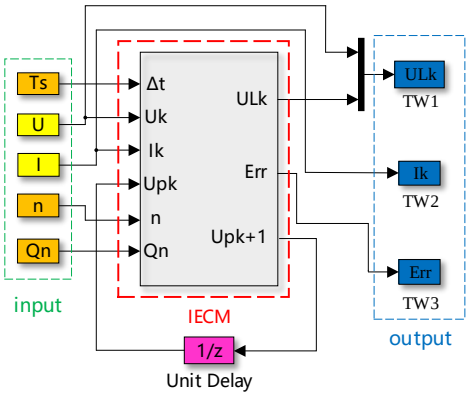

Figure 14. The parameter identification model

In Figure 14, the input parameter Δt in the model IECM is the parameter detection period, and then the closed-circuit voltage ULk and its tracking error Err of the output parameter are obtained by model operation through the open-circuit voltage [43], current and SOC parameters in the experimental process. According to the joint identification process, a parameter identification model is established to identify the parameters of the IECM model in the integrated SOC estimation process of the power LIB pack, and obtain the estimated values of the voltage and current parameters. According to the multi-input case, the unit element network module is used to obtain the battery status information, and the comprehensive SOC value can be calculated for the power LIB pack. By using the associated BMS equipment, combined with the Battery Maintenance and Testing System (BMTS) platform operating conditions simulation, the effective energy management objectives can be achieved along with the SOC value detection and evaluation process. The parameter values of the IECM model can be obtained by using the identification process, which are used to initialize the basic parameters of the power LIB pack state space equation.

4.3. Experiments and verification

In order to verify the validity of the UKF and SVM joint algorithm. Through the selection of LIB type and measurement method, the specific parameters required for LIB pack are determined as basic parameters and stopping conditions. The measurement and calculation are realized by the process from full discharge to discharge cut-off voltage, and the process of data acquisition by cyclic charging and discharging.

The Ternary LIB pack samples are selected as experimental samples for experimental research. According to the experimental requirements of parameter identification in the state space equation of the IECM model, the Hybrid Pulse Power Characterization(HPPC) experiment in the intermittent discharge process is performed by the power battery test system to obtain various model parameters and their determination rules. In order to obtain the required change rule of closed-circuit voltage output response of the power lithium ion battery pack, the power lithium ion battery pack is first fully charged through the CC-CV charging and maintenance process to make its SOC value reach 100.00% And then left to stand for half an hour to stabilize its internal electrochemical reaction, and then experimental tests are carried out. The experimental steps are as follows [44]. Charge and discharge with a constant current of 1C, first discharge the LIB for 10s, then let stand for 40s, and then charge for 10s. In the cycle test, the LIB was subjected to HPPC experiments at equally spaced (i.e., 1h) SOC points. Let the SOC be 0.1, 0.2, ... 0.9, respectively.

After several cycles of testing, the relationship between terminal voltage and time is obtained, as shown in Figure 15.

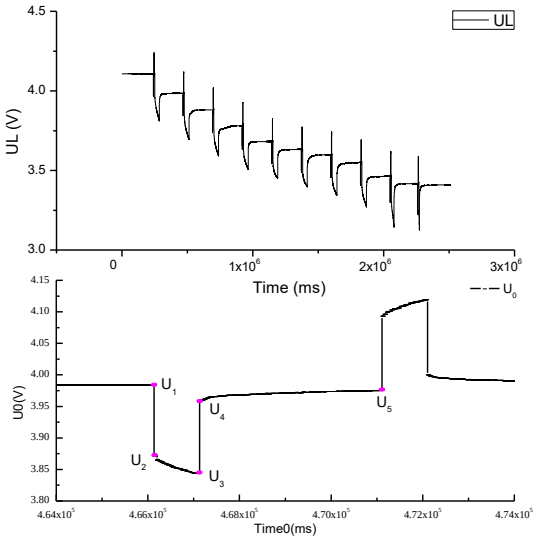

Figure 15. HPPC voltage response curve

The figure above shows the curve of the back-end voltage of the HPPC cycle charge and discharge experiment. The data of a period of time is selected for amplification, and the relationship curve of U_0 with time is obtained. Due to the effect of ohmic internal resistance, the voltages in the $U_1 \to U_2$ and $U_3 \to U_4$ processes voltages appear and rise. The reason for the $U_2 \to U_3$ process is because the RC circuit characterizes the results of the polarization effect. The $U_4 \to U_5$ stands for the shelving process. By analyzing the HPPC experimental data of the IECM model, the voltage parameter value of the equivalent circuit of the LIB at a certain SOC node can be obtained, and then the theoretical value of various parameters in the model is obtained by the characteristic equation.

After the experimental test is completed, the experimental data is imported into the simulation model, and the UKF algorithm is used to estimate the SOC. Then combine SVM with UKF algorithm. The SOC estimation effect diagram is shown in Figure 16.

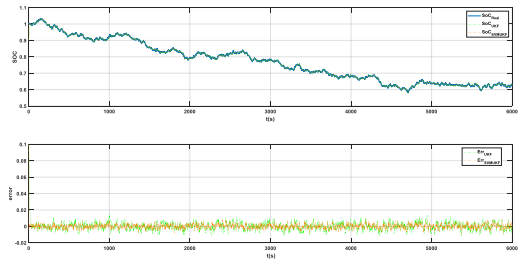

a) Overall contrast curve

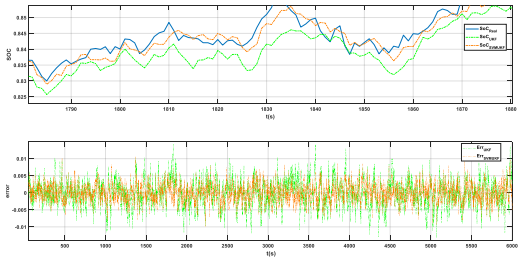

b) Partial magnification curve

Figure 16. SOC estimation comparative curves

In Figure 16, it can be seen from the figure that the error of SOC based on UKF estimation is within 3%. Then the SVM estimation method is integrated into the UKF estimation method, and the SOC estimation error is within 1%.

From the comparative analysis of Figure 16, it can be found that when SVM and UKF jointly estimate the SOC value, it greatly reduces the estimation error and can achieve high-precision estimation of SOC.

5. CONCLUSIONS

This paper mainly studies the construction method of the IECM equivalent circuit model of the power lithium battery and completes the construction of the experimental platform. By the experimental result analysis, the SOC estimation error of the designed BMS is within 1.00%. A novel equivalent model of IECM is constructed for the power LIB pack by the model equivalence analysis and characterization. According to the experimental analysis, the CCV tracking results of the equivalent model parameters for the proposed IECM battery model are verified. In the SOC estimation algorithm, a new algorithm, SVM and UKF estimation algorithm, is adopted. According to the experimental results, this method has higher estimation accuracy, and its estimation error is less than 1%, which brings

practical value to electric vehicle battery and has good reference significance for high-precision estimation of SOC.

NOMENCLATURE:
The symbols used in this research can be described as shown in Table 2.

Table 2. List of symbols

Symbol	Description	Symbol	Description
Ah	Ampere-hour	LIB	Lithium-Ion Battery
AD	Altium Designer	NN	Neural Network
BMS	Battery Management System	OCV	Open Circuit Voltage
BMTS	Battery Maintenance and Testing System	PCB	Printed Circuit Board
DCM	Discharging and Charging Maintenance	SOB	State Of Balance
EKF	Extended Kalman Filter	SOC	State Of Charge
ECM	Equivalent Circuit Model	SOH	State Of Health
EVs	Electric Vehicles	SVM	Support Vector Machine
HPPC	Hybrid Pulse Power Characterization	UKF	Unscented Kalman Filter
KF	Kalman Filter	UT	Unscented Transformation
KVL	Kirchhoff Voltage Law		

ACKNOWLEDGMENTS
This work was supported by the National Natural Science Fund of China (Grant No. 61801407) and the Undergraduate Innovation Fund Project (CX19-097).

References

1. J. Jaguemont, L. Boulon, and Y. Dubé, *Appl.Energy,* 164 (2016) 99.
2. B.M. Ge, Y.H. Liu, H. Abu-Rub, and F.Z. Peng, *IEEE Trans. Ind. Electron.*, 65 (2018) 2268.
3. A. Guha and A. Patra, *IEEE Trans. Transp. Electrif.*, 4 (2018) 135.
4. A. Ito, A. Kawashima, T. Suzuki, S. Inagaki, T. Yamaguchi, and Z.M. Zhou, *IEEE Trans. Control Syst. Technol.*, 26 (2018) 51.
5. M. Cacciato, G. Nobile, G. Scarcella, and G. Scelba, *IEEE Trans. Power Electron.*, 32 (2017) 794.
6. X.Y. Li, G.D. Fan, G. Rizzoni, M. Canova, C.B. Zhu, and G. Wei, *Energy,* 116 (2016) 154.
7. C.Z. Liu, W.Q. Liu, L.Y. Wang, G.D. Hu, L.P. Ma, and B.Y. Ren, *J. Power Sources*, 320 (2016) 1.
8. D.M. Zhou, K. Zhang, A. Ravey, F. Gao, and A. Miraoui, *Energies*, 9 (2016) 123.

9. W. Sung, D.S. Hwang, B.J. Jeong, J. Lee, and T. Kwon, *Int. J. Automot. Technol.*, 17 (2016) 493.
10. Y.J. Wang, D. Yang, X. Zhang, and Z.H. Chen, *J. Power Sources*, 315 (2016) 199.
11. Y. Merla, B. Wu, V. Yufit, N.P. Brandon, R.F. Martinez-Botas, and G.J. Offer, *J. Power Sources.*, 307 (2016) 308.
12. C.H. Piao, Z.C. Li, S. Lu, Z.K. Jin, and C. Cho, *J. Power Electron.*, 16 (2016) 217.
13. C. Goebel, H. Hesse, M. Schimpe, A. Jossen, and H.A. Jacobsen, *IEEE Trans. Power Syst.*, 32 (2017) 2724.
14. M.A. Hannan, M.S.H. Lipu, A. Hussain, M.H. Saad, and A. Ayob, *Ieee Access.*, 6 (2018) 10069.
15. X.P. Chen, W.X. Shen, M.X. Dai, Z.W. Cao, J. Jin, and A. Kapoor, *IEEE Trans. Veh. Technol.*, 65 (2016) 1936.
16. Z.B. Wei, S.J. Meng, B.Y. Xiong, D.X. Ji, and K.J. Tseng, *Appl. Energy*, 181 (2016) 332.
17. Y. Chen, X.F. Liu, Y.Y. Cui, J.M. Zou, and S.Y. Yang, *IEEE Trans. Power Electron.*, 31 (2016) 4916.
18. Y.J. Wang, C.B. Zhang, and Z.H. Chen, *J. Power Sources*, 305 (2016) 80.
19. S.L. Wang, L.P. Shang, Z.F. Li, H. Deng, and J.C. Li, *Appl. Energy,* 166 (2016) 44.
20. X.W. Guo, L.Y. Kang, Y. Yao, Z.Z. Huang, and W.B. Li, *Energies*, 9 (2016) 100.
21. H.W. He, R. Xiong, and J.K. Peng, *Appl. Energy*, 162 (2016) 1410.
22. K. Lim, H.A. Bastawrous, V.H. Duong, K.W. See, P. Zhang, and S.X. Dou, *Appl. Energy,* 169 (2016) 40.
23. E. Sarasketa-Zabala, E. Martinez-Laserna, M. Berecibar, I. Gandiaga, L.M. Rodriguez-Martinez, and I. Villarreal, *Appl. Energy,* 162 (2016) 839.
24. D. Del Testa, N. Michelusi, and M. Zorzi, *IEEE Trans. Wireless Commun.*, 15 (2016) 1393.
25. P. Wesskamp, P. Haussmann, and J. Melbert, *IEEE Trans. Instrum. Meas.*, 65 (2016) 1651.
26. J.G. Zhu, Z.C. Sun, X.Z. Wei, and H.F. Dai, *J. Appl. Electrochem.*, 46 (2016) 157.
27. L.S. Su, J.B. Zhang, J. Huang, H. Ge, Z. Li, F.C. Xie, and B.Y. Liaw, *J. Power Sources*, 315 (2016) 35.
28. X.S. Hu, S.E. Li, and Y.L. Yang, *IEEE Trans. Transp. Electrif.*, 2 (2016) 140.
29. M.A. Hannan, M.M. Hoque, S.E. Peng, and M.N. Uddin, *IEEE Trans. Ind. Appl.*, 53 (2017) 2541.
30. L.X. Liao and F. Kottig, *Appl. Soft Comput.*, 44 (2016) 191.
31. H.M. Zou, W. Wang, G.Y. Zhang, F. Qin, C.Q. Tian, and Y.Y. Yan, *Energy Convers. Manage.*, 118 (2016) 88.
32. J. Zhu, T. Wierzbicki, and W. Li, *J. Power Sources*, 378 (2018) 153.
33. L.H. Saw, Y.H. Ye, and A.A.O. Tay, *J. Cleaner Prod.*, 113 (2016) 1032.
34. M. Dubarry, A. Devie, and B.Y. Liaw, *J. Power Sources*, 321 (2016) 46.
35. G.L. Plett, *J. Power Sources*, 134 (2004) 262.
36. J. Su, M. Lin, S. Wang, J. Li, J. Coffie-Ken, and F. Xie, *Meas. Control.*, 52 (2019) 193.
37. Y. Wang, C. Zhang, and Z. Chen, *Appl. Energy.*, 185 (2017) 2026.
38. S. Tong, M.P. Klein, and J.W. Park, *J. Power Sources*, 293 (2015) 428.
39. Y. Wang, C. Zhang, and Z. Chen, *Appl. Energy.*, 137 (2015) 427.
40. J. Peng, J. Luo, H. He, and B. Lu, *Appl. Energy*, 253 (2019) 113520.
41. X. Chen, H. Lei, R. Xiong, W. Shen, and R. Yang, *Appl. Energy*, 255 (2019) 113758.
42. X. Hu, S.E. Li, and Y. Yang, *IEEE Trans. Transp. Electrif.*, 2 (2016) 140.
43. Y. Wang, C. Zhang, and Z. Chen, *J. Power Sources*, 305 (2016) 80.
44. S. Schindler, M. Bauer, M. Petzl, and M.A. Danzer, *J. Power Sources*, 304 (2016) 170.